OPEN ACCESS
IOP Publishing
Journal of Micromechanics and Microengineering
J. Micromech. Microeng. **27** (2017) 035018 (8pp)
doi:10.1088/1361-6439/aa5ae3

Fabrication and optimisation of a fused filament 3D-printed microfluidic platform

A M Tothill, M Partridge, S W James[1] and R P Tatam

Centre for Engineering Photonics, Cranfield University, Cranfield, Bedfordshire, MK43 0AL, United Kingdom

E-mail: s.w.james@cranfield.ac.uk

Received 11 October 2016, revised 5 January 2017
Accepted for publication 20 January 2017
Published 15 February 2017

Abstract

A 3D-printed microfluidic device was designed and manufactured using a low cost ($2000) consumer grade fusion deposition modelling (FDM) 3D printer. FDM printers are not typically used, or are capable, of producing the fine detailed structures required for microfluidic fabrication. However, in this work, the optical transparency of the device was improved through manufacture optimisation to such a point that optical colorimetric assays can be performed in a 50 μl device. A colorimetric enzymatic cascade assay was optimised using glucose oxidase and horseradish peroxidase for the oxidative coupling of aminoantipyrine and chromotropic acid to produce a blue quinoneimine dye with a broad absorbance peaking at 590 nm for the quantification of glucose in solution. For comparison the assay was run in standard 96 well plates with a commercial plate reader. The results show the accurate and reproducible quantification of 0–10 mM glucose solution using a 3D-printed microfluidic optical device with performance comparable to that of a plate reader assay.

Keywords: 3D-printing, microfluidics, devices, glucose, enzymatic

(Some figures may appear in colour only in the online journal)

1. Introduction

The increasing burden being placed on health care services by an aging population, obesity epidemic and diabetes epidemic [1] is creating a necessity for point-of-care testing for serious pathologies such as cardiovascular disease and diabetes [2]. New developments in economical analytical screening tools such as lab-on-a-chip [3], lab-on-a-disc [4] and microfluidic analysis systems [5] focus on miniaturisation and disposability to improve performance, speed, and portability.

The advance of solid freeform fabrication techniques, such as 3D-printing, has significantly improved the ability to prepare solid structures with precise geometries [6], including internal cavities, facilitating the rapid production of analytical platforms and the ability to alter or redesign any aspect without significantly inflating costs. The rapid advancement of low-end 3D printing technology is due largely to the development of free and open source software and hardware development [7]. In addition, there is a large library of freely available CAD models, which provides shortcuts to product development.

The ability to manufacture detailed and complex prototypes in a fast and efficient way has caused rapid prototyping technology to become a fundamental tool for many areas of research and development. Fused deposition modelling (FDM) based 3D printers are readily available for purchase either as self-assembly kits or as pre-assembled units. While the use of 3D-printing to produce cost-effective tools for biomedical applications has significant potential [8, 9], to date its use in the optical and biosensors field is limited.

Traditionally, glass and silicon have been used in the fabrication of microfluidic devices due to their well-established properties and manufacturing techniques, such as photolithography and micromachining [10]. However, more recently, the use of relatively inexpensive large scale techniques such as injection molding and hot embossing has led to an increase in the use of polymers for economical microfluidic device

[1] Author to whom any correspondence should be addressed.

Original content from this work may be used under the terms of the Creative Commons Attribution 3.0 licence. Any further distribution of this work must maintain attribution to the author(s) and the title of the work, journal citation and DOI.

 © 2017 IOP Publishing Ltd Printed in the UK

manufacturing [11]. As well as being low-cost and disposable, polymers are highly adaptable for diagnostic purposes [12]. This has resulted in materials such as polymethylmethacrylate (PMMA) and polydimethylsiloxane (PDMS) becoming highly desirable for microfluidic device prototyping [10], and for the manufacture of disposable lab equipment such as the PMMA cuvettes used in this work. While polylactic acid (PLA) is not yet commonly used as a microfluidic platform, devices have been developed [13], and PLA's biochemical properties and suitability for surface chemistry are understood [14, 15].

3D-printed optical assay platforms can suffer from the poor optical characteristics [16] of the available polymers such as PLA and acrylonitrile butadiene styrene (ABS), particularly their poor optical transparency, which is a fundamental obstacle that must be overcome for the technology to progress. In addition, FDM suffers from a large inhomogeneity between the layers and strands of plastic, which causes the formation of air pockets between strands. The distribution of small air pockets throughout the model causes scattering and attenuation of transmitted light. Other 3D printing techniques such as stereolithography and inkjet printing have higher resolution, which greatly reduces the formation of these gaps.

Chen *et al* used FDM of a proprietary acrylate-based polymer material, Vero Clear, to produce plates for use with a standard plate reader for the quantitative analysis of red blood cells for transfusion medicine. Whilst capable of printing the plates, the Objet Connex 350 Multi-material 3D printer that was used to print the devices costs over $200 000 and the devices required post-print finishing including cleaning and polishing using sand paper and water to achieve acceptable physical properties and the levels of optical transparency required for use with a standard plate reader [17]; these finishing techniques would be unsuitable for use in sealed microfluidic channels. In addition, the material used is not readily available for public use.

Dolomite FDM printers have been able to produce reliable channels of dimensions down to 300 μm using PLA plastic [18]. While the Dolomite printers are an order of magnitude cheaper than the most expansive printers, they currently cost ~£13 000 for the printer and ~£350 for the materials, which is still expensive when compared to consumer grade FDM printer prices (~£1000 and £15).

Erkal *et al* also used an Objet Connex 350 Multi-material 3D printer to produce 0.5 mm^2 microfluidic channels for use with electrodes for the detection of dopamine. Post-print techniques including sonication and scraping were required to properly form channels of the desired specification [19].

The requirement for post-print finishing techniques such as the physical removal of material and polishing to improve 3D-printed objects limits greatly the potential for the 3D printing of optical microfluidic devices, especially for the fabrication of inaccessible microfluidic channels. This emphasises the need for the development of accessible and affordable prototyping technology.

Here we demonstrate a low cost disposable microfluidic optical device designed and manufactured using single step 3D-printing technology; the device is based on a cuvette, with a path length of 500 μm and a capacity of 50 μl. Optimisation of the optical transparency of the 3D-printed plastic was also investigated using various techniques during and after manufacture. The device was used to perform an enzymatic cascade reaction for the optical quantification of glucose.

While numerous analytical procedures involving chemical and enzymatic techniques have been used within glucose assays, enzymatic methods have been the most popular due to their increased specificity and selectivity. Enzymatic methods use glucose oxidase (GlOx) to oxidize glucose to produce D-gluconic acid and hydrogen peroxide (H_2O_2); the H_2O_2 is then quantified. Wong *et al* discovered that horseradish peroxidase (HRP) catalyses the oxidative coupling of chromotropic acid (CTA) and aminoantipyrine (AAP) with hydrogen peroxide to produce a blue quinoneimine dye with high absorbance in a spectral region centred on 590 nm [20].

In this work, a glucose assay utilizing an enzymatic cascade of glucose oxidase, HRP, CTA and 4-AAP was used for the production of a blue quinoneimine dye.

$$\mathrm{D{-}Glucose} + \mathrm{H_2O} + \mathrm{O_2} \xrightarrow{\mathrm{GlOx}} \mathrm{D-Gluconic\ Acid} + \mathrm{H_2O_2}$$

$$\mathrm{Chromotropic\ acid} + 4 - \mathrm{aminoantipyrine} + 2\mathrm{H_2O_2} \xrightarrow{\mathrm{HRP}} \mathrm{quinoneminie\ dye} + 4\mathrm{H_2O}.$$

The absorbance could be measured and compared against a calibration curve giving an accurate concentration of glucose in solution. The method involves a single aqueous reagent, requires no sample pre-treatment, is reproducible, simple, specific, and uses no corrosive reagents.

The platform has been designed and manufactured using standard, readily available 3D-printing software and hardware, capable of providing results in less than 5 min, which can be read using spectrometers and photometric equipment.

2. Methods

Phosphate buffered saline (PBS, 10 mM phosphate buffer, 2.7 mM potassium chloride and 137 mM sodium chloride, pH 7.4) tablets, CTA disodium salt dihydrate (CTA), 4-AAP, isopropyl alcohol, HRP Type II essentially salt-free, lyophilized powder, 150–250 units mg^{-1} solid (using pyrogallol) (HRP), D-glucose, glucose oxidase from *Aspergillus niger* lyophilized, powder, and ~200 units mg^{-1} protein (GlOx), were purchased from Sigma-Aldrich (Poole, UK). Ultrapure water (18 MΩ cm^{-1}) was produced using a Milli-Q water system (Millipore Corp., Tokyo, Japan). The concentration of glucose in samples was tested and quantified independently using an Optium Exceed Blood Glucose Monitoring System (Abbott, UK).

2.1. Glucose assay optimisation

The glucose assay consists of using an enzymatic cascade to produce a blue dye with an absorbance correlating to glucose concentration. The reagents which combine to produce the dye are CTA and 4-AAP. According to the reaction proposed by Wong *et al*, H_2O_2 reacts with CTA and AAP in the presence of HRP [20] with a molar ratio of CTA:AAP for maximum

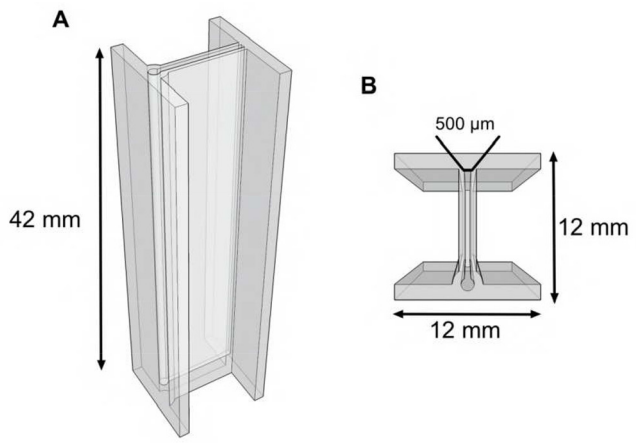

Figure 1. Schematic of the microfluidic device [22].

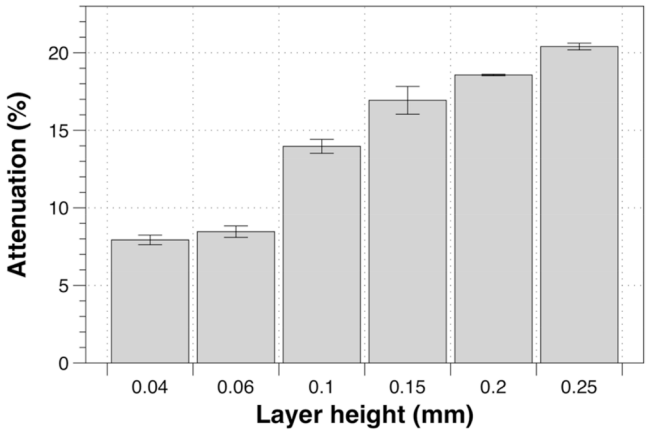

Figure 2. Attenuation at 633 nm in 400 μm thick plastic samples of ultimaker PLA translucent made with six different layer heights, $n = 3$, error bars are the standard deviation of the repeats [23].

colour produced being 5:1. It is necessary that the concentrations of CTA and AAP are sufficient to quantify accurately the substrate within the required detection range (0–10 mM). It was determined that a concentration ratio of 2:1 CTA:AAP was required for a substrate detection range of 0–10 mM glucose.

It should be noted, that although a 1:1 CTA:AAP ratio should be sufficient, the concentration of CTA must be in excess of that of AAP to prevent AAP dimerization. In the CTA/AAP reaction, CTA is oxidised by HRP producing CTA radicals. The CTA radicals then react with AAP to produce AAP radicals and CTA. The AAP radicals then react with CTA radicals in solution and H_2O_2 to produce blue quinoneimine dye. By increasing the AAP in the reagent mixture, the probability of direct oxidation of AAP by oxidised HRP is increased, which then increases the concentration of aminyl radicals and subsequently the probability of their dimerization [21]. The result of this is a decreased concentration of blue quinoneimine dye and an increased concentration of AAP dimers. By maintaining a high concentration of CTA with respect to AAP, the blue dye reaction pathway is enhanced.

Glucose assay reagent solution was made by dissolving CTA, 4-AAP, glucose oxidase (0–50 units ml^{-1}) and HRP (0–10 units ml^{-1}) in the PBS solution. The reaction was started by adding the glucose solution (up to a final concentration range of 0–10 mM). The assay was read after 2 min incubation and the absorption spectrum recorded.

Serial dilution matrices were performed for CTA (0–80 mM) and 4-AAP (0–80 mM) using 6 U ml^{-1} HRP and 10 U ml^{-1} glucose oxidase (GlOx). The reaction was started by adding 0–10 mM glucose solution. Concentration curves were produced (see the supplementary data) to determine the optimum concentration values for enzyme and reagents.

Glucose oxidase and HRP concentrations were determined using a fixed time method as this is more applicable in most clinical assays. Serial dilutions were performed of GlOx (0–50 U ml^{-1}) and HRP (0–10 U ml^{-1}) using CTA 20 mM and AAP 10 mM. The reactions were started by adding a 10mM glucose solution. The assay was incubated for 2 min and the absorbance was then measured. Samples were allowed to incubate for a further 3 min and the absorbance was measured again.

A Varioskan Flash spectral scanning multimode reader (ThermoScientific LTD, UK) was used in conjunction with the PC software package SkanIt to determine the absorbance values of the assays. Assay optimisation was carried out in Nunc-Immuno MaxiSorp flat bottom 96 well plates (Sigma-Aldrich, UK).

2.2. Fabrication of 3D-printed microfluidic device and 3D printed samples

The primary stages involved in making a 3D printed product are the creation of a CAD file, conversion and preparation of the file using a slicer program, uploading the file to the printer and finally the physical creation of the object. All 3D printed models were fabricated using an Ultimaker 2 + 3D printer using a 0.4 mm nozzle size. The accuracy of the printer in the *X*, *Y* and *Z* dimensions is 12.5, 12.5 and 5 μm respectively. The nozzle size of 0.4 mm limits the positioning of features close to each other but still allows for the design and construction of features (such as channels) of dimensions down to approximately 20 μm. However, while it is possible to create channels with this resolution, currently their formation is not reliable, and working at this scale would require improvements to the consistency of the plastic extrusion.

A number of different batches and makes of transparent filaments were used. The filaments tested include: Ultimaker PLA Translucent, Ultimaker PLA Transparent, Innofil PLA Natural and InnoPET Natural.

For this work, two different 3D models were designed. The first was a square of Ultimaker PLA Translucent plastic 20 mm^2 with 400 μm thickness and path length. The second was a 12 × 12 × 42 mm cuvette which has an internal microfluidic cavity with a thickness of 500 μm, this design is shown in figure 1. The circular tube to one side is included to allow for the total filling of the cavity. Multiple cuvettes were made from the variety of plastic filaments mentioned previously.

When printed, the measured thickness of the cavity was 480 μm. This was measured using an Olympus light microscope (model) in three locations along the length of the cavity. The measurement had an error of ±10 μm.

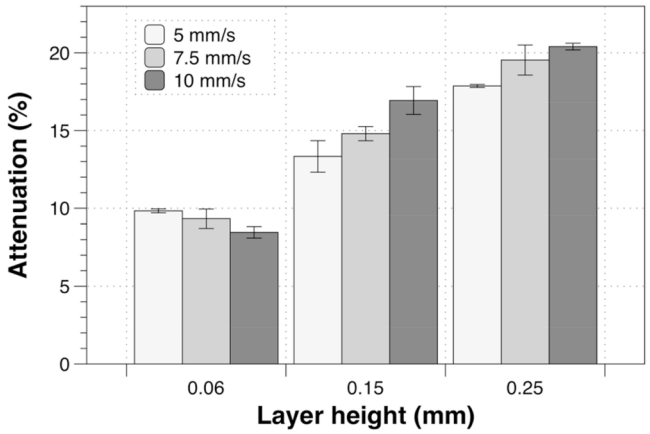

Figure 3. Attenuation in Ultimaker PLA translucent plastic samples made with three different layer heights at three different speeds, $n = 3$, error bars are the standard deviation of the repeats [24].

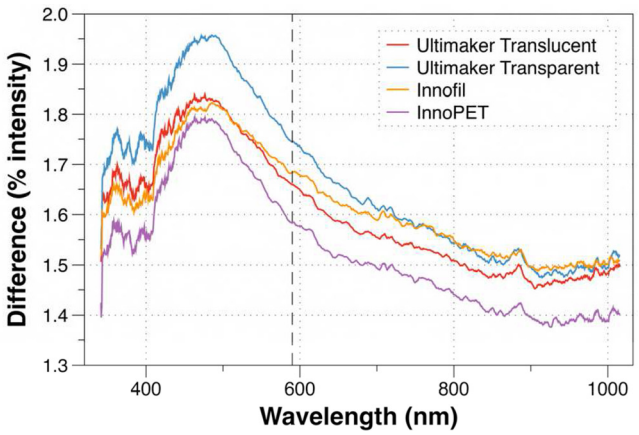

Figure 4. Difference as a percentage of intensity in the spectra of 3D printed cuvette devices compared to a PMMA cuvette [25].

Both models were designed using the 3D-modelling CAD software Sketchup 2015 Pro (Trimble Navigation Ltd, USA). The device file was converted to an STL file and processed using the slicer program Cura (Ultimaker Ltd, Netherlands). Cura was also used to calibrate and optimise the print parameters by adjusting layer height and print speed.

2.3. Glucose assay in 3D-printed microfluidic device

Glucose assay reagent solution was made by dissolving CTA (up to a final concentration of 20 mM), 4-AAP (up to a final concentration of 10 mM), glucose oxidase (20 units ml^{-1}) and HRP (6 units ml^{-1}) in a PBS solution. The reaction was started by adding glucose solution (up to a final concentration of 0–10 mM). The assay was read after a 2 min incubation and the absorption spectrum recorded. The assay was performed in a microfluidic device and the absorbance spectra assessed using the equipment described in section 2.5.

2.4. Instrumentation used to measure attenuation

Instrumentation was assembled to quantify the optical attenuation of the 3D-printed plastic samples. Plastic samples were mounted at a fixed distance in front of a Newport 1825-C Optical Power Meter (Newport, USA). The sample was then illuminated with a helium–neon laser (Uniphase, UK), operating at 633 nm and with an output power of 0.8 mW and fitted with a beam expander to create a beam waist of 20 mm. The attenuation of the sample was recorded as the difference between the transmitted power with and without the sample under test.

2.5. Spectral analysis instrumentation

The absorbance of the substrate assay reaction in the 3D-printed microfluidic devices was quantified by analysing the transmission spectrum of the assay using a fibre coupled tungsten halogen light source (Ocean Optics ecoVis, Ocean Optics, USA) and a CCD spectrometer Ocean Optics ADC1000-USB spectrometer (Ocean Optics, USA). The light source has an integrated cuvette holder which was adapted to hold the microfluidic devices. The light source and the spectrophotometer were connected using a short length (10 cm) of multimode optical fibre.

3. Results and discussion

The investigation of the use of 3D printed plastics for microfluidic devices had two key aims. Firstly, the optimisation of the 3D printing methodology to produce plastic samples of sufficient optical quality to allow the optical interrogation of internal cavities. Secondly, the demonstration of filling and reading a biological assay within a 3D printed microfluidic device.

Optimisation of the 3D printing methodology focussed on both the printing layer height and the speed of the plastic deposition. Once optimised the device repeatability was also demonstrated.

Prior to running a colorimetric glucose assay the microfluidic device, an optimisation process was undertaken to first develop a reliable glucose assay protocol and then produce a dilution curve by running the assay in a commercial well plate which was subsequently read with a commercial plate reader system.

3.1. The effect of print speed and layer height on optical transparency

As previously discussed, many factors can influence a 3D-printed object; it can take several print attempts and varying conditions to produce an object with the desired properties. The FDM printer used here deposits layers of polymer on top of each other to build up the object. The influence of these layers' height on the attenuation of the transmitted light was investigated by characterising 3D-printed solid plastic samples as described in 2.4. These samples were fabricated at 10 mm s^{-1} with varying layer heights of the plastic. The total thickness of the object was unchanged; only the height of the layers (and therefore the number of layers) was altered.

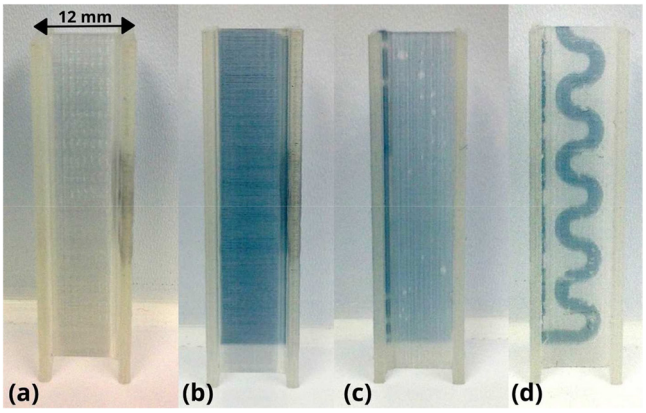

Figure 5. Microfluidic cuvette before (a) and after (b) quinoneimine dye reaction. Also shown are a microfluidic cuvette prepared with a 100 μm thick chamber (c) and an S-shaped channel (d).

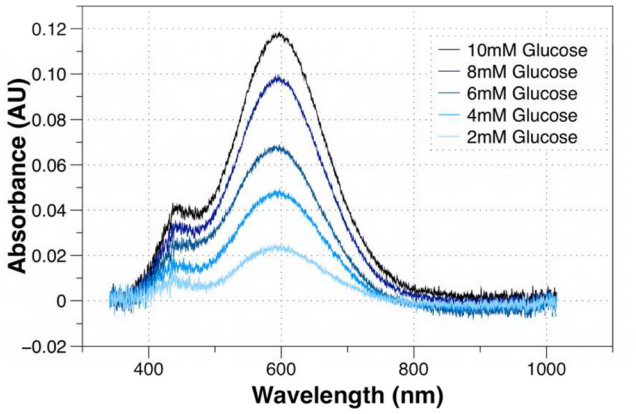

Figure 6. Change in the absorbance spectra with glucose concentration [27].

Table 1. Summary table showing intra filament % coefficient of variance (CV).

Filament type	CV between devices ($n = 3$) (%)
Ultimaker translucent	4
Ultimaker transparent	7
Innofil	4
InnoPET	3

As demonstrated in figure 2, an increase in the layer height increases the attenuation of the transmitted light. However, at 0.04 and 0.06 mm layer heights the difference between the attenuation measurements was less than the experimental error.

As layers are deposited, air can be trapped between the layers, reducing homogeneity. Such air pockets and the corresponding reduction in the merging of the polymer layers is thought to be responsible for the clouding observed in the printed samples and the measured reduction in optical transparency. Where homogeneity between layers was improved, it was observed by eye that the optical transparency increased, even if intermittently and not through the entire object. It could expected that increasing layer height would increase the optical transparency, as there are fewer layers and therefore less potential for air gaps, however it is proposed that as the layer height increases the circular nature of the FDM extruded plastic, causing the air pockets to become larger, decreasing optical transparency.

A proposed solution to the formation of air gaps was to vary the print speed to allow the plastic time to flow into the gaps. However, as shown in figure 3, the variation of the print speed had a mixed impact on the attenuation caused by the Ultimaker PLA Translucent plastic samples. For 0.06 mm layer height, the increased speeds appeared to reduce the attenuation slightly. Whereas layer heights of 0.15 and 0.25 mm showed a slight increase in attenuation with speed. In all cases the change is small and is less than 10% of the overall attenuation.

Further experiments at a wider range of speeds were attempted but this increased the failure rate of the prints. It has been documented that at higher print speeds the chance of print failure increases. This is due to the increased risk of the print not sticking to the bed, overheating, layer shifting and misalignment, grinding of the filament leading to interruption of the feed, and increased vibrations impacting the quality of fine details. This results in either incomplete, inadequate quality or aborted prints.

3.2. Device variability

To investigate the repeatability of the optical properties of the 3D printed devices, microfluidic devices were manufactured from a selection of transparent PLA filaments as described in section 2.2. Three devices were produced from each filament so that the inter and intra-filament variability could be observed. The difference in the spectra of multiple devices ($n = 3$) made from the same filament were compared using the equipment described in section 2.5 and the resulting average spectra are presented in figure 4. Each device was read a total of five times. In this data the spectra of a PMMA cuvette was used as the reference in order to highlight the spectral differences between the commercial PMMA material and the 3D printed samples.

The spectra shown all have a similar form. All of the plastic filaments show around a 15% increase in the 390 to 700 nm region and around a 10% decrease in from 700 to 1000 nm. The Innofil Natural and Ultimaker Translucent plastics have less absorbance in the 390 to 700 nm range and appear to have decreased absorbance in the 700 to 1000 nm range.

At the 590 nm absorbance peak of the quinoneimine dye the inter-filament coefficient of variance (CV) was less than 1% and there was a maximum CV of 2.6% between 390–700 nm. The intra-filament CVs are shown in table 1, where the transmission spectrum of each device was recorded a total of five times and averaged.

For a device to be used as an assay platform, reproducibility is imperative; any optical differences between 3D-printed devices could have an impact on the quantified data leading to inaccurate conclusions. While the spectral data showed good reproducibility between absorbance profiles of devices made from the same filament batch, the large differences observed between filament batches require that a filament specific calibration curve is used for each batch of filament to maximise the accuracy of quantitative data produced in each device.

Using an optical coherence tomography (OCT) instrument (Spectral Radar OCT, Thorlabs, Germany), the characteristics of three channels of depth 400 μm and width 1000 μm were

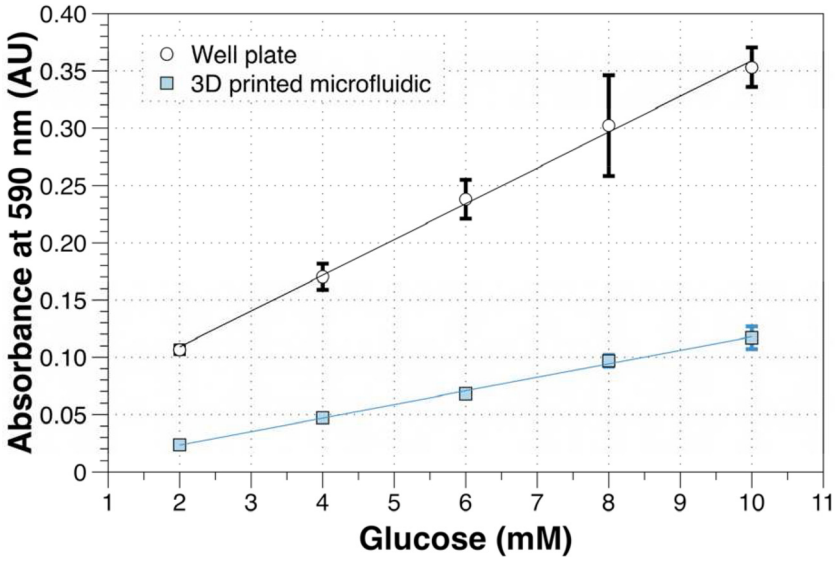

Figure 7. Absorbance at 590 nm comparison between 3D printed microfluidic and well plate reader. Error bars on all points represent three standard deviation of three repeats [28].

investigated. OCT is a low coherence interferometry technique that can be used to measure the optical thickness of layers within semi-transparent materials with a resolution on the micron scale [26]. From the OCT images it was possible to assess the surface roughness of the internal channels. Each channel was assessed at four locations, revealing a surface roughness of 135 μm with an average standard deviation of 53 μm. It is thought that one of the largest contributing factors in the roughness is the nozzle size of the plastic extruder (in this case 400 μm). The features most predominant in the OCT images were 400 μm wide plastic strands sitting slightly above the line of the adjacent strands. Future work will explore the improvement of surface roughness using smaller nozzles, of diameter down to 125 μm, which are also supported by the Ultimaker FDM printer.

3.3. Glucose assay optimisation

Optimisation experiments for the glucose assay were performed in 96 well plates using the chemical and enzyme concentrations and equipment described in section 2.1.

Glucose oxidase and HRP concentrations were determined using a fixed time method as this is more applicable in most clinical assays. In all cases, blue quinoneimine dye was produced and visible immediately with the colour intensity increasing as GlOx or HRP concentration increased. In the absence of GlOx or HRP no blue dye was produced. As 1 U corresponds to the amount of enzyme which oxidizes 1 μmol D-glucose to D-gluconolactone and H_2O_2 per minute at pH 7.0 and 25 °C, 20 U ml^{-1} GlOx should ensure a fast reaction rate ($\leqslant$2 min) with tolerances for pH and temperature fluctuations [26]. It was determined that enzyme concentrations of GlOx 20 U ml^{-1} and HRP 6 U ml^{-1} would be sufficient for an assay capable of quantifying accurately a biologically relevant glucose range of 0–10 mM with a reaction time of 2 min (data not shown). Reaction rates can be increased by increasing enzyme concentrations accordingly.

3.4. Glucose assay performed in 3D-printed microfluidic device

The microfluidic devices manufactured for use with the glucose assay were printed at a rate of 10 mm s^{-1} with a layer height of 0.06 mm using Ultimaker Translucent. The glucose assay was performed in the 3D-printed device as described in section 2.3. Samples were prepared using the chemical and enzyme concentrations described in section 2.2. The reaction was started by adding glucose solution of the desired concentration. Figure 5 shows a photograph the microfluidic channel before and after the quinoneimine dye reaction. Additionally, figure 5 shows a microfluidic cuvette manufactured with a 100 μm thick fluid cavity and a cuvette with a 500 μm thick S-shaped channel. These are included to show the range of designs possible using of 3D printing.

The absorbance spectra of the 500 μm thick single chamber microfluidic (figure 5(b)) cuvette were recorded using the methodology described in section 2.5. The resulting spectra are shown in figure 6.

As the glucose concentration increases, the quinoneimine dye concentration also increases, resulting in an increase in absorbance centred around 590 nm. The spectra produced illustrate the range over which absorbance can be quantified, providing flexibility in the wavelength, which may be used for quantitative purposes. In this work, the absorbance of quinoneimine dye was quantified at 590 nm. The approximate peak absorbance of the quinoneimine dye, for the full range of glucose concentrations are shown in figure 7, alongside the data from previous plate reader based experiments.

The data shown in figure 7 demonstrates that it is possible to measure glucose concentration using a colourimetric assay in a 3D-printed PLA device. The data produced shows a linear dilution curve for increasing glucose concentrations with an *R*-squared of 0.99. When compared to results produced with a commercial plate reader assay, the 3D-printed microfluidic device performs well. There is around a 20–30% difference in attenuation, which is consistent with the native attenuation of

the 3D-printed plastic, which reduces the sensitivity as shown in figure 3. The limits of detection of the well plate and the printed microfluidic devices were determined to be 0.12 and 0.03 mM, respectively. The lower limit of detection for the 3D printed microfluidics is due to the lower error between reps compared to the well plate.

4. Conclusions

A colorimetric glucose assay capable of distinguishing between a range of glucose concentrations (0–10 mM) in PBS pH 7.4 solution has been used to demonstrate the capability and functionality of the printed devices. The glucose assay was performed in a 3D-printed microfluidic device and absorbance data was gathered during testing that shows that it is possible to quantify colorimetric assay data in a 3D-printed device. The use of an enzymatic cascade demonstrates how a multistage assay process can be performed within the device as a single user step.

It has previously been thought that the poor optical transparency of 3D–printed polymers is a fundamental obstacle that considerably limits their potential to fabricate optically interrogated devices [16]. Furthermore, the variability and error in low cost FDM printers was thought to limit their use in fabricating microfluidic structures. When acetone vapour treatment [29] was used, it was possible to improve the transparency of plastic samples by a further 30%. While not applicable to microfluidics this highlights that for some applications it is possible to further improve the sensitivity and surface quality of devices manufactured using cheap 3D-printers with simple post-processing techniques.

Additionally, more expensive 3D-printing techniques have higher resolution and better accuracy, which can also improve the optical properties of the plastic. However, these systems can cost as much as $200 000, which is beyond the budget of many research laboratories and would make the cost of individual sample holders prohibitive in many applications.

The microfluidic device demonstrated in this paper was manufactured using an Ultimaker 2 + FDM printer costing $2000, using filament purchased from the Ultimaker website for $30–$50 per 750 gram reel. Each device cost 3–10¢ depending on the filament used, when compared to purchasing standard disposable PMMA cuvettes which cost approximately 7¢ each, resulting in an economical device that can be custom designed and built to the users' requirements without having to wait for purchasing or delivery. Further investigation is to be performed into secondary adsorption phenomena that may influence the analytical spectroscopy and reproducibility of data involving 3D-printed PLA devices however the use of PLA in biochemical devices is already established [14,15].

Whilst many industrial microfluidic devices are produced using injection molding, this is a very costly production method for research labs [30] as each design change can cost as much as $3000 to have the molds made. The use of 3D-printing in device fabrication would allow researchers to prototype various microfluidic systems quickly and cheaply, both reducing the cost and time for development of a microfluidic platform. 3D printing also allows for structures and shapes that are not possible in injection molding and could open up new 3D designs in microfluidics. This includes the inclusion of electrodes and other devices into the 3D printed structure. This is something we have already begun exploring with simple electrode systems and fibre optic sensors.

In future work we will look at complex microfluidic structures as well as the flow dynamics of 3D-printed surfaces. It is also envisaged that this will expand into testing the suitability of this approach for blood and urine analysis and further develop in to complex 3D-printed devices such as lab-on-a-disc assay platforms providing mobile diagnostic information efficiently and cheaply for personal health monitoring.

Acknowledgments

The authors acknowledge funding from the Engineering and Physical Sciences Research Council (EPSRC) UK, via grants EP/N002520 and EP/H02252X. The underlying data can be found on the Cranfield Online Research Data repository using the links provided in the reference list.

References

[1] NICE 2010 *Cardiovascular Disease Prevention* (PH25) (available at https://www.nice.org.uk/guidance/ph25) (accessed 07/02/2017)

[2] Tang W H W, Francis G S, Morrow D A, Newby L K, Cannon C P, Jesse R L, Storrow A B, Christenson R and HNACB Committee 2008 National academy of clinical biochemistry laboratory medicine practice guidelines: clinical utilization of cardiac biomarker testing in heart failure *Clin. Biochem.* **41** 210–21

[3] Mirasoli M, Guardigli M, Michelini E and Roda A 2014 Recent advancements in chemical luminescence-based lab-on-chip and microfluidic platforms for bioanalysis *J. Pharm. Biomed. Anal.* **87** 36–52

[4] Arnandis-Chover T, Morais S, González-Martínez M Á, Puchades R and Maquieira Á 2014 High density microarrays on Blu-ray discs for massive screening *Biosens. Bioelectron.* **51** 109–14

[5] Livak-Dahl E, Sinn I and Burns M 2011 Microfluidic chemical analysis systems *Annu. Rev. Chem. Biomol. Eng.* **2** 325–53

[6] Hutmacher D W, Sittinger M and Risbud M V 2004 Scaffold-based tissue engineering: rationale for computer-aided design and solid free-form fabrication systems *Trends Biotechnol.* **22** 354–62

[7] Zhang C, Anzalone N C, Faria R P and Pearce J M 2013 Open-source 3D-printable optics equipment *PLoS ONE* **8** e59840

[8] Cohen D L, Malone E, Lipson H and Bonassar L J 2006 Direct freeform fabrication of seeded hydrogels in arbitrary geometries *Tissue Eng.* **12** 1325–35

[9] Ballyns J J, Cohen D L, Malone E, Maher S A, Potter H G, Wright T, Lipson H and Bonassar L J 2010 An optical method for evaluation of geometric fidelity for anatomically shaped tissue-engineered constructs *Tissue Eng. Part C Methods* **16** 693–703

[10] Ansari M I H, Hassan S, Qurashi A and Khanday F A 2016 Microfluidic-integrated DNA nanobiosensors *Biosens. Bioelectron.* **85** 247–60

[11] Becker H and Locascio L E 2002 Polymer microfluidic devices *Talanta* **56** 267–87
[12] Siegrist J, Gorkin R, Bastien M, Stewart G, Peytavi R, Kido H, Bergeron M and Madou M 2010 Validation of a centrifugal microfluidic sample lysis and homogenization platform for nucleic acidextraction with clinical samples *Lab. Chip* **10** 363–71
[13] Zhao Y, Leung L, Naguib H and You L 2009 Microfluidics chamber system for bone cell mechanotransduction study and bone tissue engineering application *55th Annual Meeting of the Orthopaedic Research Society*
[14] Pioggia G, Di Francesco F, Marchetti A, Ferro M and Ahluwalia A 2007 A composite sensor array impedentiometric electronic tongue Part I. Characterization *Biosens. Bioelectron.* **22** 2618–23
[15] Kadimisetty K, Mosa I M, Malla S, Satterwhite-Warden J E, Kuhns T M, Faria R C, Lee N H and Rusling J F 2016 3D-printed supercapacitor-powered electrochemiluminescent protein immunoarray *Biosens. Bioelectron.* **77** 188–93
[16] Willis K, Brockmeyer E, Hudson S and Poupyrev I 2012 *Printed Optics: 3D Printing of Embedded Optical Elements for Interactive Devices* (New York: ACM)
[17] Chen C, Wang Y, Lockwood S Y and Spence D M 2014 3D-printed fluidic devices enable quantitative evaluation of blood components in modified storage solutions for use in transfusion medicine *Analyst* **139** 3219–26
[18] Bhattacharjee N, Urrios A, Kang S and Folch A 2016 The upcoming 3D-printing revolution in microfluidics *Lab Chip* **16** 1720–42
[19] Erkal J L, Selimovic A, Gross B C, Lockwood S Y, Walton E L, McNamara S, Martin R S and Spence D M 2014 3D printed microfluidic devices with integrated versatile and reusable electrodes *Lab. Chip* **14** 2023–32
[20] Wong R C, Ngo T T and Lenhoff H M 1981 Formation of blue chromophore from oxidative coupling of aminoantipyrine with chromotropic-acid in the presence of peroxide and horseradish-peroxidase *Int. J. Biochem.* **13** 159–63
[21] Nicell J A and Wright H 1997 A model of peroxidase activity with inhibition by hydrogen peroxide *Enzyme Microb. Technol.* **21** 302–10
[22] Tothill A 2016 *BIOS2016 P2.006 Microfluidic Device (500 μm)* (online) (www.thingiverse.com/thing:1558265) (Accessed: 12th May 2016)
[23] Tothill A 2016 3D printed plastic attenuation with layer height (figshare) Retrieved: 06 49, 6 October 2016 (GMT) (doi: 10.17862/cranfield.rd.3443639.v1)
[24] Tothill A 2016 3D printed plastic attenuation with print speed (figshare) Retrieved: 06 49, 6 October 2016 (GMT) (doi: 10.17862/cranfield.rd.3363049.v1)
[25] Tothill A 2016 Percentage intensity difference of transparent 3D plastics (figshare) Retrieved: 06 49, 6 October 2016 (GMT) (doi: 10.17862/cranfield.rd.3443645.v1)
[26] Wilson R and Turner A P F 1992 Glucose oxidase: an ideal enzyme *Biosens. Bioelectron.* **7** 165–85
[27] Tothill A 2016 Absorbance spectra of microfluidic cuvette glucose sensor (figshare) Retrieved: 06 49, 6 October 2016 (GMT) (doi: 10.17862/cranfield.rd.3443648.v1)
[28] Tothill A 2016 Absorbance of 3D printed microfluidic biosensor at 590nm (figshare) Retrieved: 06 49, 6 October 2016 (GMT) (doi: 10.17862/cranfield.rd.3443651.v1)
[29] Naga N, Yoshida Y, Noguchi K and Murase S 2013 Crystallization of amorphous poly(lactic acid) induced by vapor of acetone to form high crystallinity and transparency specimen *Open J. Polym. Chem.* **2013** 29–33
[30] Fiorini G S and Chiu D T 2005 Disposable microfluidic devices: fabrication, function, and application *BioTechniques* **38** 429–46

https://dspace.org/

Fabrication and optimisation of a fused filament 3D-printed microfluidic platform

Tothill, Alexander M.; Partridge, Matthew; James, Stephen W.; Tatam, Ralph P.

2017-02-15
IOP Publishing
https://doi.org/10.1088/1361-6439/aa5ae3
Tothill A, Partridge M, James SW, Tatam R. (2017) Fabrication and optimisation of a fused filament 3D-printed microfluidic platform. Journal of Micromechanics and Microengineering, Volume 27, Issue 3, March 2017, Article number 035018

Downloaded from a DSpace repository. https://dspace.org/